Prevailing Surface Wind Direction during Air–Sea Heat Exchange

FUMIAKI OGAWA AND THOMAS SPENGLER

Geophysical Institute, University of Bergen, and Bjerknes Centre for Climate Research, Bergen, Norway

ABSTRACT

While the climatological-mean sensible and latent heat fluxes are remarkably well described using climatological-mean fields in the bulk flux formulas, this study shows that a significant fraction of the climatological-mean wind speed in the midlatitudes is associated with wind variations on synoptic time scales. Hence, the prevailing wind direction associated with the most intense air–sea heat exchange can differ from the mean wind direction. To pinpoint these striking differences between the climatological and synoptic viewpoint, this study presents a global climatology of the prevailing surface wind direction during air–sea heat exchanges calculated for instantaneous and time-averaged reanalysis data. The interpretation of the fluxes in the lower latitudes is basically unaffected by the different time averages, highlighting the time-mean nature of the circulation in the lower latitudes. In the midlatitudes, however, the prevailing wind direction features a significant equatorward component for subweekly time averages and reverts to pure westerlies for longer time averages. These findings pinpoint the necessity to consider subweekly time scales, in particular along the midlatitude SST fronts, to describe the air–sea heat exchange in a physically consistent way.

1. Introduction

The crucial role of air–sea heat exchange in the global energy cycle demands a physical understanding and sound interpretation of the distribution of surface sensible and latent heat fluxes. Because the climatological-mean fluxes are well described using time-mean fields in the bulk flux formulas (Simmonds and Dix 1989), many studies employ stationary and linear thinking to describe the response to sea surface temperature (SST) anomalies and fronts in the low latitudes (Lindzen and Nigam 1987; Wallace et al. 1989) as well as extending similar paradigms to the midlatitudes (Minobe et al. 2008, 2010; Lambaerts et al. 2013). However, recent studies challenge the notion that the climatological mean in the midlatitudes is physically well described by the time-mean fields and argue to consider fluctuations on subweekly synoptic time scales to explain the climatological-mean features (Czaja and Blunt 2011; Parfitt and Czaja 2016; O'Neill et al. 2017; Vanniere et al. 2017a; Parfitt and Seo 2018). This is also reflected by the fact

that the 10-m mean wind speed ($\overline{w}_{10} = \overline{|\mathbf{u}_{10}|}$) is generally not identical to the 10-m wind speed based on the mean wind components ($\overline{w}_{10} \neq |\overline{\mathbf{u}}_{10}| = \sqrt{\overline{u}_{10}^2 + \overline{v}_{10}^2}$). The inequality also implies that the prevailing wind direction is not equal to the mean wind direction. Motivated by these disagreements, we assess the role of synoptic-scale eddies for the prevailing wind direction associated with air–sea heat exchange.

Most air–sea interaction paradigms are inspired by atmospheric flow in the low latitudes considering steady-state linear theory, where the role of eddies is not explicitly considered. For example, Lindzen and Nigam (1987) and Wallace et al. (1989) addressed the influence of tropical SST anomalies and fronts on the surface winds using monthly mean data. Xie (2004) discussed the atmospheric circulation in the lower troposphere in response to SST anomalies on time scales well beyond subweekly atmospheric synoptic eddies. However, since the transient eddy activity is relatively weak in the low latitudes, it can be argued that the monthly mean fields approximately describe the physical nature of the air–sea interaction.

Corresponding author: Fumiaki Ogawa, fumiaki.ogawa@uib.no

While the mean easterlies in the low latitudes are ascribed to the rather steady trade winds, the surface westerlies in the midlatitudes are associated with the eddy-driven jet, which is less apparent in instantaneous wind fields (e.g., Hartmann 1994; Vallis 2017). This contrast is also evident in the character of the mean atmospheric meridional overturning mass circulation. While it is mainly associated with the Eulerian time-mean Hadley circulation with its trade winds in the low latitudes, it is dominated by baroclinic eddies in the midlatitudes (e.g., Vallis 2017). The dominance of these baroclinic eddies in the midlatitudes in fact leads to a reversal of the Eulerian mean thermally indirect Farrell cell to the hemispherically thermally direct meridional overturning circulation of mass (e.g., Peixoto and Oort 1992; Vallis 2017). In the low latitudes, on the other hand, the Eulerian time-mean is associated with the thermally direct Hadley circulation with its trade winds. With the midlatitude mean flow being so strongly influenced by eddies, one would expect significant ramifications for the surface flow and thus air–sea heat exchange.

Moreover, these baroclinic eddies are most active in the vicinity of midlatitude SST fronts, accompanied by high-frequency meridional winds (Nakamura et al. 2004; Ogawa et al. 2012). The meridional wind advects cold and dry air over the warm western boundary currents, correspondingly causing high-frequency fluctuation and variance of the upward surface fluxes in these regions (Zolina and Gulev 2003; Nonaka et al. 2009; Taguchi et al. 2009; Tilinina et al. 2018). These fluxes, on the other hand, contribute significantly to the enhanced development of these baroclinc cyclones (e.g., Hoskins and Hodges 2002; Brayshaw et al. 2009; Booth et al. 2010, 2012; Czaja and Blunt 2011). The result of these mutual interactions is also hypothesized to anchor the midlatitude storm tracks along the SST fronts (Sampe et al. 2010; Hotta and Nakamura 2011).

For the Gulf Stream SST front, O'Neill et al. (2017) showed that the accumulated effect of strong baroclinic cyclones largely explains the climatological-mean precipitation and near-surface divergence/convergence of low-level wind along the Gulf Stream region. This is in contrast to Minobe et al. (2008), who argued for the significance of the low-level convergence via the mean fields. Other recent studies pinpointed to the effect of atmospheric fronts associated with baroclinic cyclones to play a crucial role for the air–sea heat exchange, where the role of cold fronts prevails over that of warm fronts (Vanniere et al. 2017a, b). Cold fronts, and their impact on air–sea heat exchange, are sensitive to the underlying structure in the SST front (Parfitt et al. 2016) and contribute significantly to the low-level convergence (Parfitt and Seo 2018).

Overall, the recent emphasis on the contribution of synoptic-scale fronts and cyclones to the air–sea heat exchange in the midlatitudes challenges the use of linear steady-state thinking in these regions. The contrast between the climatological time-mean westerlies and the significant meridional eddy flow poses the question if the physical interpretation of the air–sea heat exchange along midlatitude SST fronts by the mean wind is appropriate. In the low latitudes, on the other hand, the circulation is largely dominated by the mean flow and the interpretation is thus more straightforward. To analysize these differences between the lower and middle latitudes, we assess the prevailing wind direction for air–sea heat exchange for the entire globe and pinpoint where the mean wind components or eddies dominate, respectively.

2. Data

We use the European Centre for Medium-Range Weather Forecasts (ECMWF) interim reanalysis (ERA-Interim; Dee et al. 2011) for the period 1979–2015. The data are available at 0.75° resolution with a 6-hourly time interval providing analyses at 0000, 0600, 1200, and 1800 UTC. We interpolated the data onto a 0.5° grid and use the 10-m zonal (u_{10}) and meridional (v_{10}) wind components, temperature (T_2) and dewpoint (T_{d2}) at 2 m, sea surface temperature (SST), sea ice concentration, as well as surface sensible (SSHF) and latent heat fluxes (SLHF). We use T_{d2} to calculate specific humidity (q_2) at 2 m. The surface fluxes at the four analysis times were derived using the accumulated surface fluxes from the 0000 UTC (1200 UTC) ERA-Interim forecasts between +3 and +9 as well as +9 and +15 to calculate the 0600 and 1200 UTC (1800 and 0000 UTC) analysis, respectively.

We calculated daily, weekly, and monthly means based on the 6-hourly data and derived annual as well as seasonal means for December–February (DJF) and June–August (JJA). In our analyses, we mask out regions where the climatological-mean sea ice concentration exceeds 30%. A recent study pinpointed the impact of a resolution change in the SST in ERA-Interim reanalysis after 2002 (Masunaga et al. 2015). Our results, however, are qualitatively not affected by this change in resolution and remain robust over the entire data period. Furthermore, repeating our analysis using a different reanalysis dataset (JRA-55; Kobayashi et al. 2015), we obtain the same result.

3. Decomposing the wind and the role of eddies

Using the bulk formulas SSHF $\propto w_{10}\Delta T$ and SLHF $\propto w_{10}\Delta q$, we can derive the time mean:
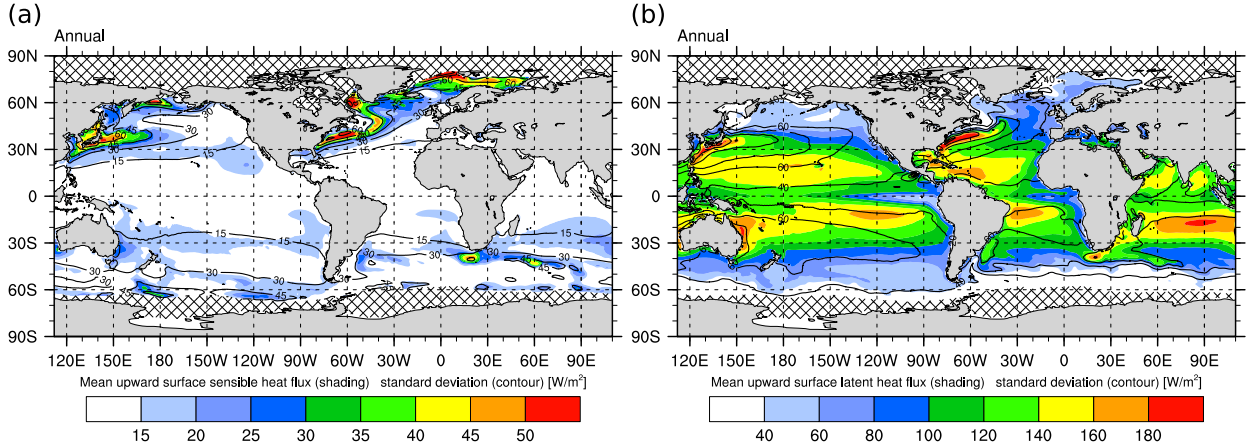
FIG. 1. Mean upward surface (a) sensible and (b) latent heat flux (W m^{-2}; shading) and their standard deviation (W m^{-2}; contours). The hatched mask indicates where the climatological-mean sea ice concentration exceeds 30%.

$$\overline{\text{SSHF}} \propto \overline{w_{10}\Delta T} = \overline{w}_{10}\overline{\Delta T} + \overline{w_{10}^*\Delta T^*} + \overline{w_{10}'\Delta T'} + \overline{w_{10}^*\Delta T'} + \overline{w_{10}'\Delta T^*}$$
$$\approx \overline{w}_{10}\overline{\Delta T} + \overline{w_{10}^*\Delta T^*} + \overline{w_{10}'\Delta T'} \tag{1}$$

and

$$\overline{\text{SLHF}} \propto \overline{w_{10}\Delta q} = \overline{w}_{10}\overline{\Delta q} + \overline{w_{10}^*\Delta q^*} + \overline{w_{10}'\Delta q'} + \overline{w_{10}^*\Delta q'} + \overline{w_{10}'\Delta q^*}$$
$$\approx \overline{w}_{10}\overline{\Delta q} + \overline{w_{10}^*\Delta q^*} + \overline{w_{10}'\Delta q'}, \tag{2}$$

with 10-m wind speed $w_{10} = (u_{10}^2 + v_{10}^2)^{1/2}$ as well as air–sea temperature difference $\Delta T = \text{SST} - T_2$ and specific humidity $\Delta q = q_{\text{sat}_{\text{SST}}} - q_2$ difference, where $q_{\text{sat}_{\text{SST}}}$ is saturation specific humidity at SST. We separated variables as $f = \overline{f} + f^* + f'$, with time mean $\overline{f}$, seasonal variations defined as the 30-day running mean f^*, and submonthly eddies f'. A quantitative check confirmed that the cross correlations $\overline{f^*g'}$ are negligible (one order of magnitude smaller than the other terms). The cross terms $\overline{f^*g'}$ would be larger if we use a 10-day running mean to define f^*, although still negligibly small relative to the other terms. Thus, our main arguments are qualitatively not affected by our choice of a 30-day running mean.

There is a large resemblance of $\overline{\text{SSHF}}$ and $\overline{\text{SLHF}}$ (Fig. 1) by $\overline{w_{10}\Delta T}$ and $\overline{w_{10}\Delta q}$ (Figs. 2a,b), giving credence to the approximations in Eqs. (1) and (2). Figures 2a and 2b also show that $\overline{w}_{10}\overline{\Delta T}$ and $\overline{w}_{10}\overline{\Delta q}$ explain more or less 100% of $\overline{w_{10}\Delta T}$ and $\overline{w_{10}\Delta q}$, respectively, on almost the entire globe. The dominance of the mean term persists even when considering the variation of the heat transfer coefficients in the bulk formulas (not shown). Hence, the eddy ($\overline{w_{10}'\Delta T'}$, $\overline{w_{10}'\Delta q'}$) and seasonal ($\overline{w_{10}^*\Delta T^*}$, $\overline{w_{10}^*\Delta q^*}$) covariances contribute very little to the approximation of $\overline{\text{SSHF}}$ and $\overline{\text{SLHF}}$. The insignificance of $\overline{w_{10}'\Delta T'}$ and $\overline{w_{10}'\Delta q'}$ can be explained by considering the fact that $\overline{|v_{10}'|\Delta T'}$ and $\overline{|v_{10}'|\Delta q'}$ cancel for alternating southerly and northerly flow associated with opposing air–sea temperature differences (not shown).

Thus, the global distribution of $\overline{\text{SSHF}}$ and $\overline{\text{SLHF}}$ is largely determined by the mean air–sea temperature difference $\overline{\Delta T}$ and specific humidity difference $\overline{\Delta q}$ (Figs. 2c,d) as well as the mean wind speed $\overline{w}_{10}$ (Fig. 3a). The large $\overline{\text{SSHF}}$ along the major SST fronts in the midlatitudes as well as along the sea ice edge (Fig. 1a) can thus be readily explained by the large $\overline{\Delta T}$ in these regions (Fig. 2c) being aligned with significant $\overline{w}_{10}$ (Fig. 3a). Similarly, $\overline{\text{SLHF}}$ can be explained by the saturation deficit in the subtropical latitudes as well as along the midlatitude SST fronts (Fig. 2d) in conjunction with the mean wind speed in these areas (Fig. 3a). While the dominance of the mean terms might be surprising at first, it should be noted that $\overline{\Delta T}$ and $\overline{\Delta q}$ stem from an asymmetric probability density distribution with a long one-sided tail that is most likely associated with eddies (not shown). We do not further address this nonlinear eddy contribution to the mean terms, because it does not affect our arguments within this study.

While the interpretation of $\overline{\Delta T}$ and $\overline{\Delta q}$ is linear and thus straightforward, the interpretation of $\overline{w}_{10}$ is more involved. In comparing $\overline{u}_{10}$ and $\overline{v}_{10}$ with $\overline{w}_{10}$ (Fig. 3a), it is evident that $\overline{w}_{10} \approx (\overline{u}_{10}^2 + \overline{v}_{10}^2)^{1/2}$ over large parts of the low latitudes, whereas $\overline{w}_{10} \neq (\overline{u}_{10}^2 + \overline{v}_{10}^2)^{1/2}$ in the extratropics. To address this discrepancy we rewrite and separate

$$\overline{w}_{10}^2 + \overline{w_{10}^{*2}} + \overline{w_{10}'^2} \approx \overline{u}_{10}^2 + \overline{v}_{10}^2 + \overline{u_{10}^{*2}} + \overline{v_{10}^{*2}} + \overline{u_{10}'^2} + \overline{v_{10}'^2}, \tag{3}$$

where cross terms $\overline{f'f^*}$ were again negligible (one order of magnitude smaller than the other terms). With $\overline{w}_{10}^2$ being the dominant left-hand-side term (>80% almost
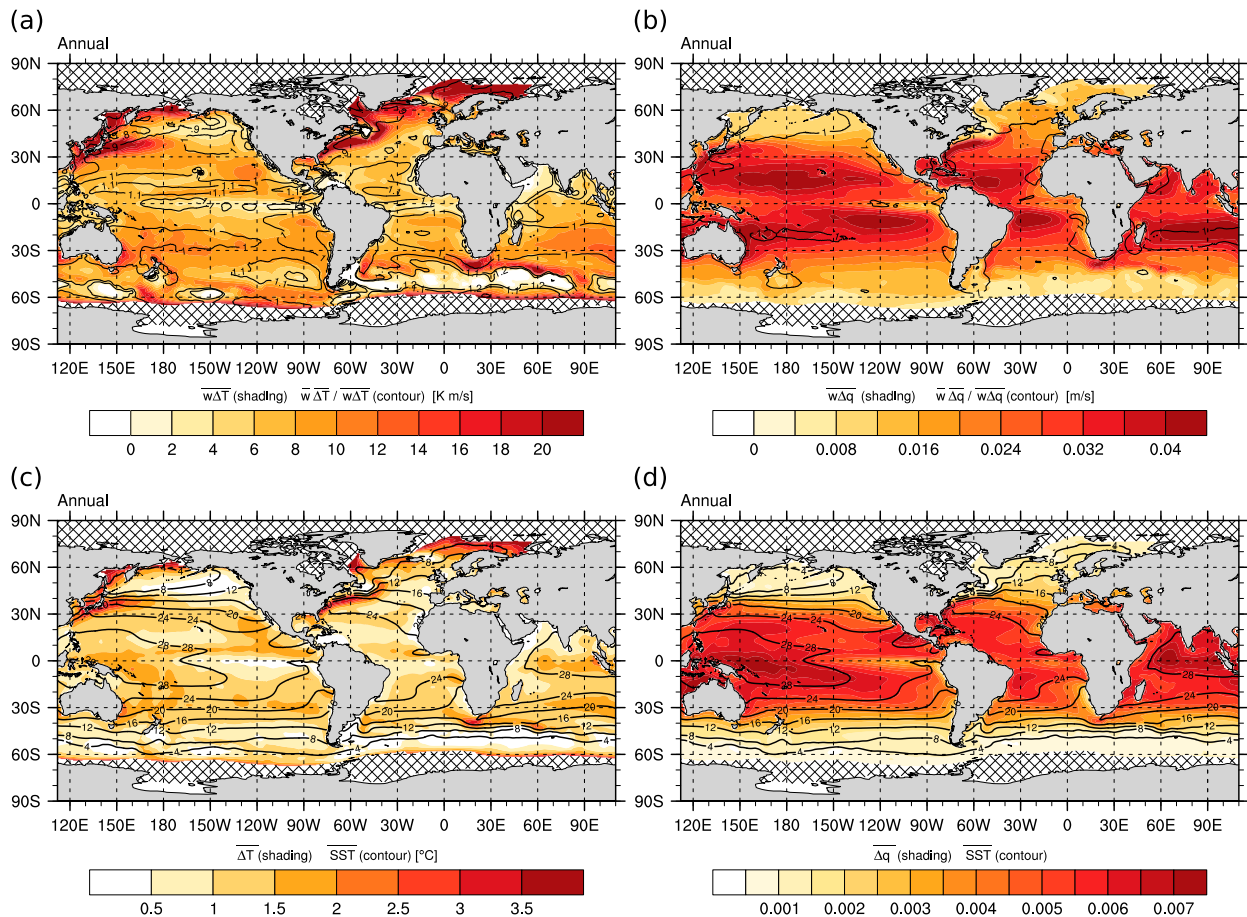
FIG. 2. Mean contributions to the bulk flux formula for (a) sensible heat flux $\overline{w}_{10}\overline{\Delta T}$ (K m s^{-1}; shading) and ratio $\overline{w}_{10}\overline{\Delta T}/\overline{w_{10}\Delta T}$ (contours, not shown where the denominator is less than 0.1) and (b) latent heat flux $\overline{w}_{10}\overline{\Delta q}$ (m s^{-1}; shading) and ratio $\overline{w}_{10}\overline{\Delta q}/\overline{w_{10}\Delta q}$ (contours). Also shown are (c) mean temperature difference $\overline{\Delta T}$ between SST and 2-m temperature (K; shading) and $\overline{SST}$ (K; contours) and (d) mean specific humidity difference $\overline{\Delta q}$ between 2-m specific humidity and saturation humidity at SST (g kg^{-1}; shading) and again $\overline{SST}$ (K; contours).

everywhere on the globe; Fig. 3c), we interpret each term on the right-hand side as a contribution to $\overline{w}_{10}$.

In the low latitudes, $(\overline{u}_{10}^2 + \overline{v}_{10}^2)$ explains over 80% of $\overline{w}_{10}^2$ (Fig. 3d). In the midlatitudes, however, $(\overline{u}_{10}^2 + \overline{v}_{10}^2)$ only explains up to 10% (Fig. 3d). The seasonality terms $(\overline{u_{10}^{*2} + v_{10}^{*2}})$ are small, with the only appreciable exception being the tropical regions of the Asian and Australian monsoon (Fig. 3e). The resulting void in the midlatitudes is filled by the eddies $(\overline{u_{10}^{\prime 2} + v_{10}^{\prime 2}}$; Fig. 3f), which contribute about 80% to $\overline{w}_{10}^2$.

It is noteworthy that the eddy contribution is larger equatorward of the SST front (see Fig. 3f), while $\overline{w}_{10}^2$ maximizes more along the SST front (Fig. 3a). While the core of the storm track features stronger mean zonal flow $\overline{u}_{10}$, synoptic eddies, in particular their cold fronts, sway farther equatorward of the main storm track region (Berry et al. 2011) enhancing the relative contribution of the eddy wind component there.

This analysis is consistent with the previously stated fact that $\overline{w}_{10} \approx (\overline{u}_{10}^2 + \overline{v}_{10}^2)^{1/2}$ in the low latitudes (Figs. 3a,d), where the means of the directional wind components contribute most to the mean wind. In contrast $\overline{w}_{10} \neq (\overline{u}_{10}^2 + \overline{v}_{10}^2)^{1/2}$ in the midlatitudes, where the eddies are dominant (Fig. 3f), with meridional and zonal eddy components contributing almost equally (Fig. 3b, black and blue contours). It is noteworthy that the SST front collocates with the maxima of $\overline{v_{10}^{\prime 2}}$ (Fig. 3b), consistent with the strong synoptic eddy activity along the SST front (e.g., Nakamura et al. 2004; Ogawa et al. 2012). With $\overline{\Delta T}$ and $\overline{\Delta q}$ (Figs. 2c,d) maximizing along the equatorward flank of the SST front, a significant contribution to $\overline{SSHF}$ and $\overline{SLHF}$ is thus associated with $\overline{v_{10}^{\prime 2}}$. Hence, despite the directional mean wind being westerlies, a dominant fraction of the maximum mean fluxes in the vicinity of SST fronts is attributable to the meridional eddy wind.
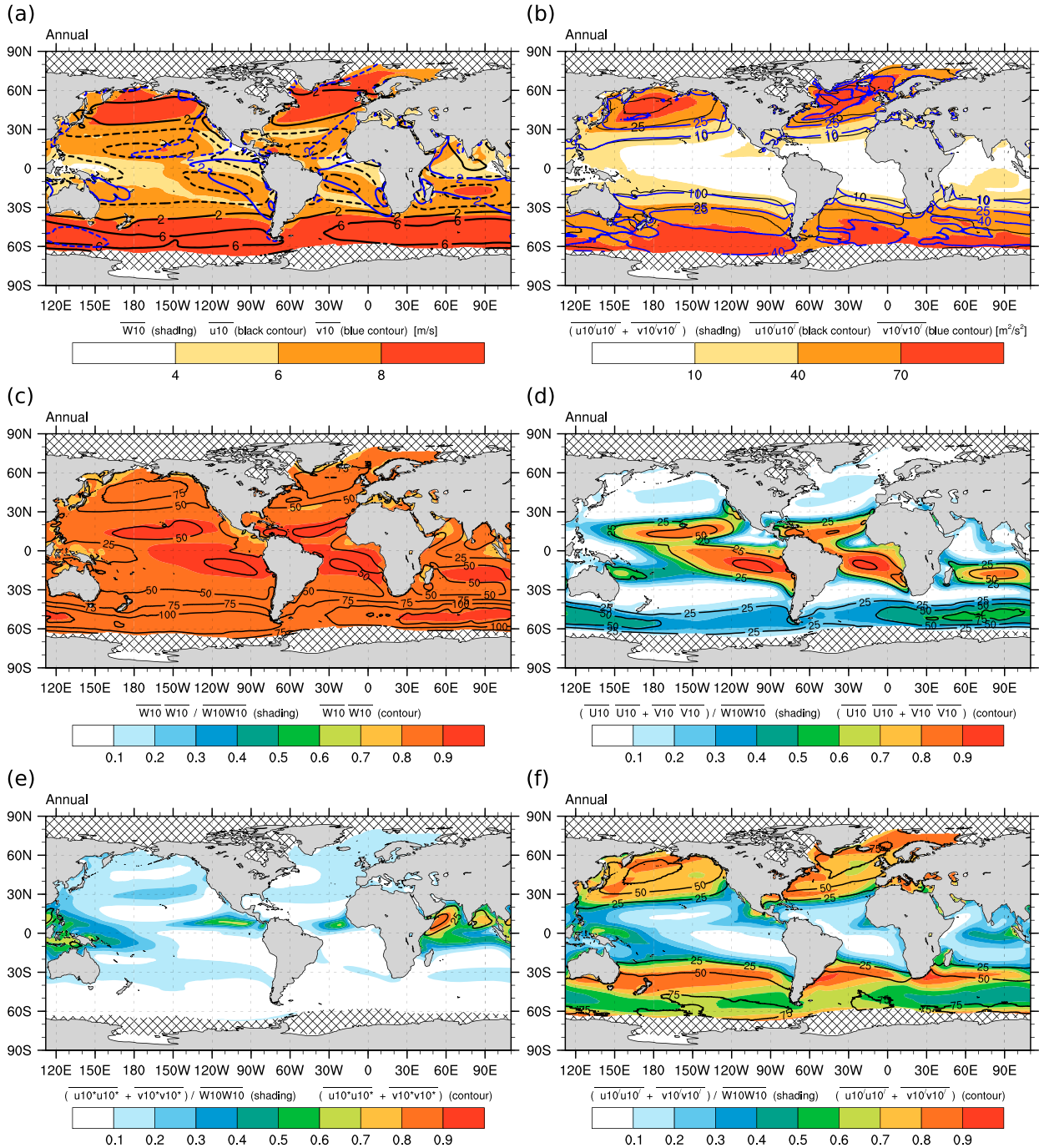
FIG. 3. Decomposition of the mean wind: (a) mean wind $\overline{w}_{10}$ (m s^{-1}; shading) and mean wind components $\overline{u}_{10}$ (m s^{-1}; black contours) and $\overline{v}_{10}$ (m s^{-1}; blue contours), (b) mean eddy wind $(\overline{u_{10}'^2} + \overline{v_{10}'^2})$ (m^2 s^{-2}; shading) and eddy wind components $\overline{u_{10}'^2}$ (m^2 s^{-2}; black contours) and $\overline{v_{10}'^2}$ (m^2 s^{-2}; blue contours), (c) ratio $\overline{w}_{10}^2/\overline{w_{10}^2}$ (shading) and $\overline{w_{10}^2}$ (m^2 s^{-2}; contours), and ratio for (d) mean wind components $(\overline{u}_{10}^2 + \overline{v}_{10}^2)/\overline{w_{10}^2}$ (shading), (e) seasonal wind components $(\overline{u_{10}^{*2}} + \overline{v_{10}^{*2}})/\overline{w_{10}^2}$ (shading), and (f) eddy wind components $(\overline{u_{10}'^2} + \overline{v_{10}'^2})/\overline{w_{10}^2}$ (shading), with the sum of the means of the respective wind components (contours).

4. Wind direction associated with surface fluxes

To further address this mismatch of mean wind direction associated with surface fluxes, we accumulatively bin upward SSHF and SLHF into eight wind directions (north, northeast, east, southeast, south, southwest, west, and northwest). Thus, the sum over all eight bins yields the total upward SSHF and SLHF, respectively.

We perform this binning for the 6-hourly as well as the daily, weekly, and monthly mean data for each grid point in the ERA-Interim reanalysis for the period 1979–2015. Figures 4a–d and 5a–d exemplarily illustrate the binned results for SSHF based on the different time-averaged data for grid points in the North Atlantic Ocean averaged along 55°–45°W at 15° and 40°N, respectively.

The tropical grid points (Figs. 5a–d) exhibit no dependence on the different time averaging of the data, with mainly easterly flow associated with SSHF in this area. There is a slight indication of a northeasterly flow component for 6-hourly and daily mean data, though the overall picture is very consistent among the four different time averages. This consistency is attributable to the stable trade winds and associated dominance of the mean wind components in these latitudes (Fig. 3d). The grid points just equatorward of the Gulf Stream SST front (Figs. 4a–d), however, feature a large sensitivity to the time averaging of the data. While the weekly and monthly mean is dominated by westerlies, the daily and 6-hourly data have a large imprint of northwesterlies. The discrepancy between the two locations resembles the previous results, with the dominance of the mean wind components in the low latitudes and the dominance of the eddies in the midlatitudes. The transition of the prevailing wind direction from northwesterly to westerly between daily (Fig. 4b) and weekly (Fig. 4c) time scales is found for the 2-day mean (not shown). This time scale is consistent with the passage of a typical flow field of a regular-sized cyclone.

At 40°N, almost $500\,\mathrm{MJ\,yr^{-1}}$ are associated with northwesterlies when using 6-hourly data, whereas only about $250\,\mathrm{MJ\,yr^{-1}}$ are associated with westerlies. For the monthly mean data, however, the northwesterlies are only associated with slightly more than $125\,\mathrm{MJ\,yr^{-1}}$ and the westerlies feature more than $750\,\mathrm{MJ\,yr^{-1}}$. Thus, the difference in these wind components is by a factor of 4 and 3, respectively. Considering the orientation of the SST front in this area, these differences in wind direction have significant ramifications for the physical interpretation of the fluxes. While the 6-hourly data feature a significant wind component across the SST front (the orientation of the SST front is indicated by the black line; Figs. 4a–d), the monthly mean data indicate that almost all fluxes are associated with westerlies.

As the midlatitude SST fronts are collocated with the storm tracks (e.g., Nakamura et al. 2004; Ogawa et al. 2012), the equatorward eddy flow across the SST front is largely associated with synoptic-scale baroclinic eddies and cold air outbreaks (Papritz and Spengler 2015) that move cold and dry air masses equatorward.

These displacements of air masses lead to significant $\overline{\Delta T}$ and $\overline{\Delta q}$ along the equatorward flanks of the SST fronts (see Figs. 2c,d), yielding large surface fluxes along the Gulf Stream and Kuroshio (Fig. 1). Interestingly, the most frequent wind direction in the midlatitude North Atlantic for 6-hourly and daily data is not equatorward but southwesterly (Figs. 4e,f). For weekly and monthly mean data, however, the dominant wind direction shifts more to westerlies (Figs. 4g,h). While the wind speed is similar for all wind directions and time scales (Figs. 4i–l), the air–sea temperature difference ΔT is much larger for wind directions crossing the SST front (Figs. 4m–p).

The prevailing wind direction for the air–sea heat exchange (Figs. 4a–d) is a convolution of the wind direction (Figs. 4e–h) and the wind direction associated with air–sea temperature differences (Figs. 4m–p). Thus, the dominant fluxes associated with northwesterlies for 6-hourly and daily data for air–sea heat exchange (Figs. 4a–b) can be explained mainly by the dominance of the air–sea temperature difference for northerly flow (Figs. 4m–n). On the other hand, the prevailing westerlies for weekly and monthly mean data for air–sea heat exchange (Figs. 4c,d) are mainly due to the dominance of the westerlies and the absence of significant air–sea temperature differences for southwesterly wind (Figs. 4o,p).

While the air–sea heat exchange is associated with cross-SST-front wind for both 6-hourly and daily as well as weekly and monthly mean data, the physical interpretation differs significantly. For 6-hourly and daily data, synoptic-scale activity associated with the passage of atmospheric fronts (Parfitt and Seo 2018) and cold air outbreaks (Papritz and Spengler 2015) together with the orientation of the SST front yield an adequate physical interpretation of the mean fluxes in these regions. On the other hand, the weekly and monthly mean data imply an association of the mean surface westerlies with the air–sea heat exchange.

In the lower latitudes, on the other hand, the dominant wind direction (Figs. 5e–h) and highest wind speed (Figs. 5i–l) are easterly regardless of the averaging time scale. However, there is no preference in wind direction for ΔT (Figs. 5m–p), yielding easterlies as the prevailing wind direction for air–sea heat exchange in the lower latitudes (Figs. 5a–d).

5. Dominant wind direction for surface fluxes

To further pinpoint differences in the interpretation of the wind direction associated with surface fluxes, we present a global analysis indicating the wind direction at each grid point for which the largest accumulated
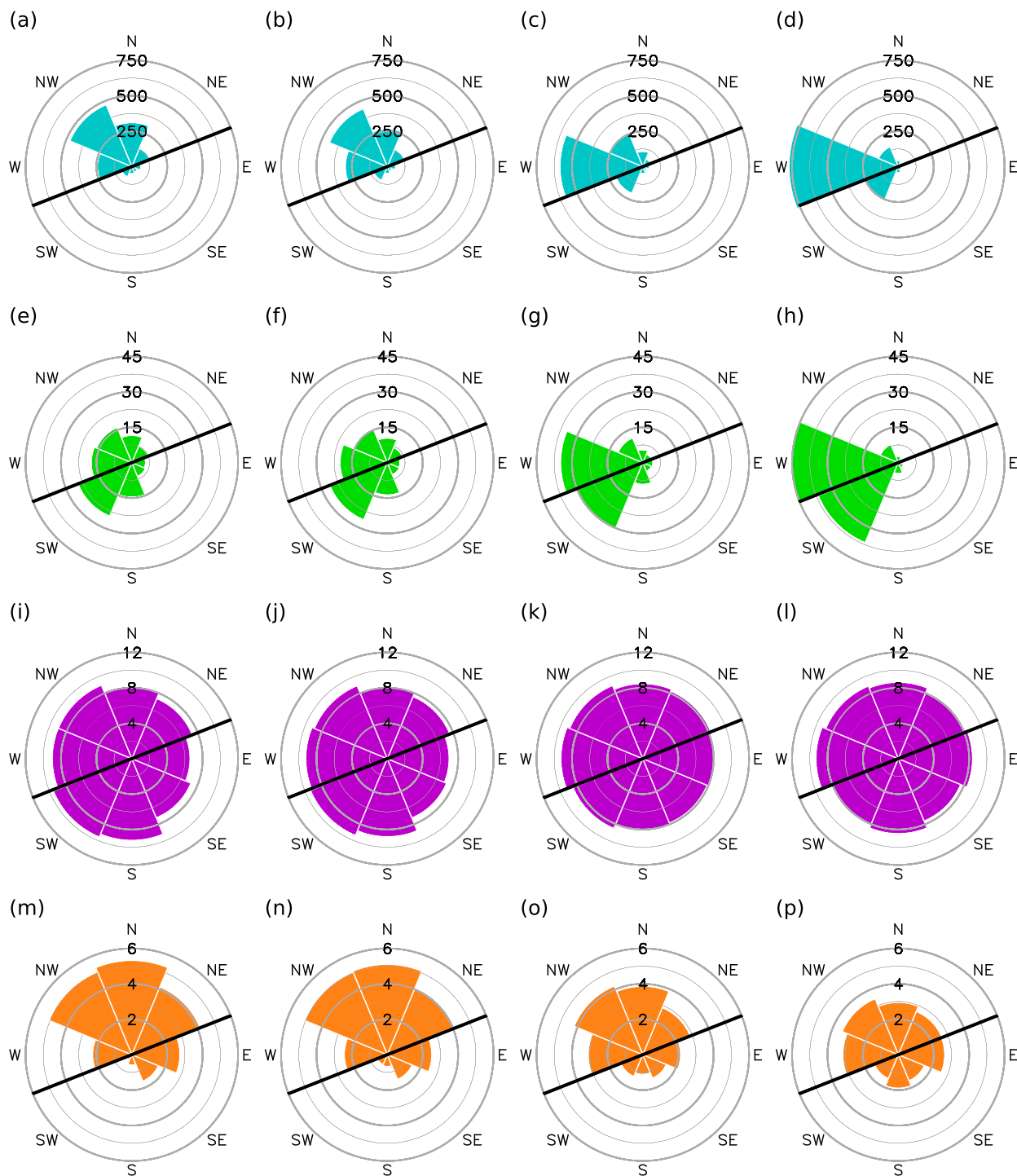
FIG. 4. All data binned for the eight wind directions: (a)–(d) Integrated upward surface sensible heat flux (MJ yr^{-1}), (e)–(h) probability of the wind direction (%), (i)–(l) $\overline{w}_{10}$ (m s^{-1}) and (m)–(p) $\overline{\Delta T}$ (K) for (left) 6-hourly, (left center) daily mean, (right center) weekly mean, and (right) monthly mean data for grid points equatorward of the Gulf Stream SST front at 40°N, 55°–45°W. The thick black line indicates the orientation of the SST front.
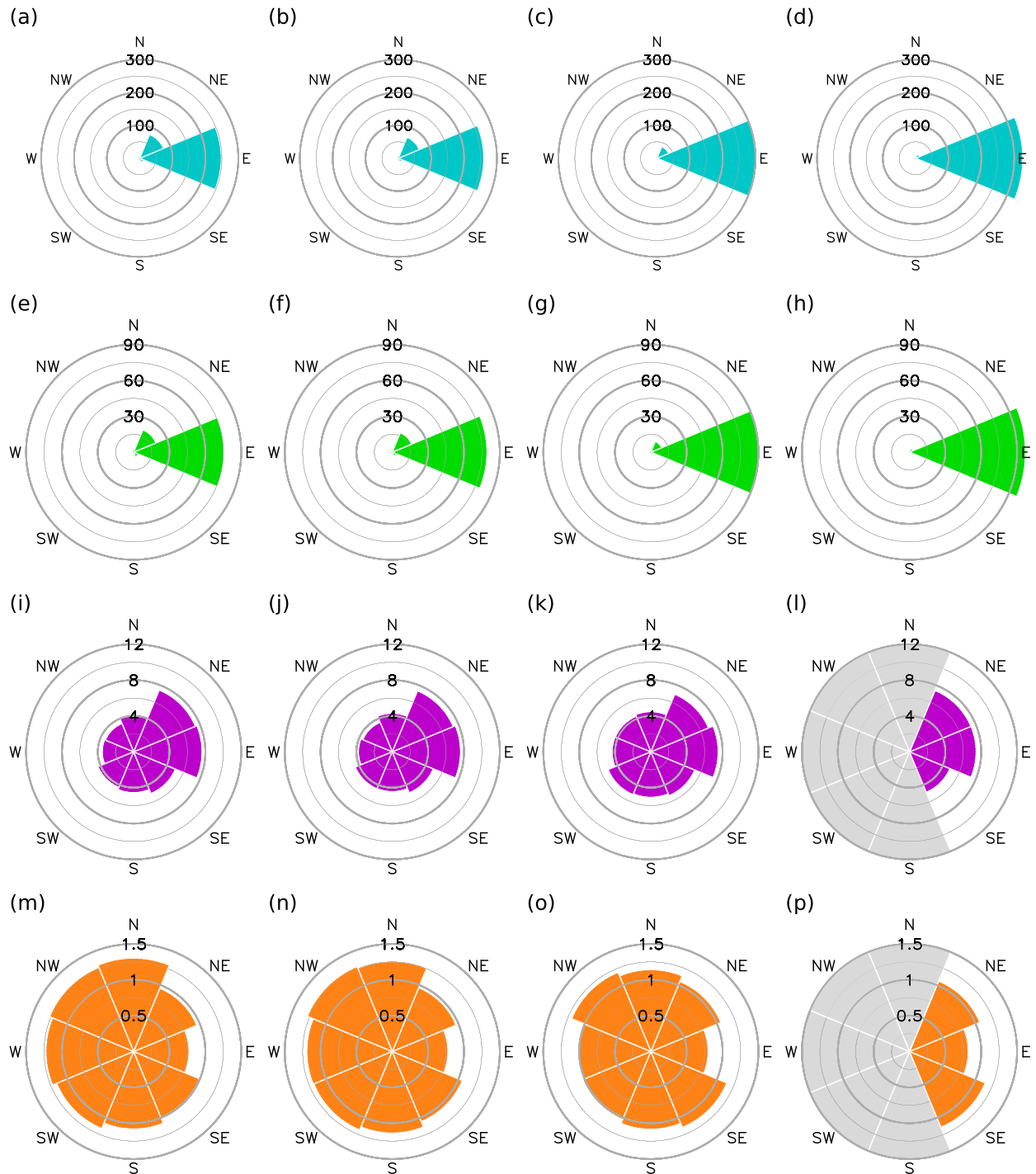
FIG. 5. As in Fig. 4, but for a grid point in the tropics at 15°N, 55°–45°W. Gray shading indicates that there are no counts of the corresponding wind direction.

SSHF or SLHF were identified. As 6-hourly and daily mean as well as weekly and monthly mean data bear great resemblance, respectively (see Fig. 4), we limit our presentation to results for 6-hourly and monthly mean data.

a. Annual mean

The dominant wind directions using monthly mean data for SSHF (Fig. 6b) and SLHF (Fig. 6d) are mostly zonal. The ratio of the heat flux explained by the wind
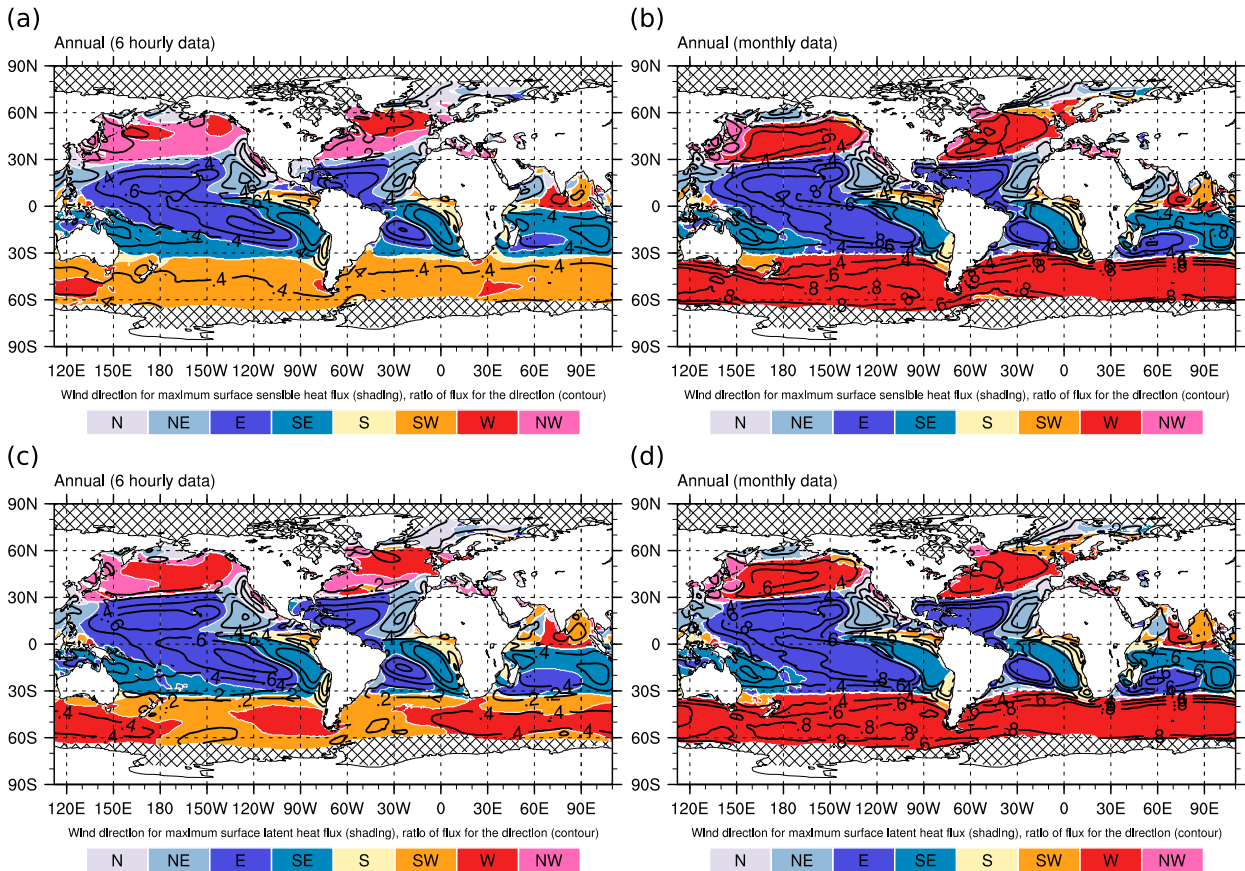
FIG. 6. Prevailing wind direction for integrated surface (a),(b) sensible and (c),(d) latent heat flux for (left) 6-hourly and (right) monthly mean data. Contours depict the ratio between accumulated and total fluxes in the indicated wind direction.

direction is ~80% and ~60% in the tropical and midlatitude region, respectively (contours in Figs. 6b,d). The dominance of the easterlies in the lower latitudes is associated with the mean trade wind. The South Pacific convergence zone (e.g., Vincent 1994) features southeasterlies, while the tropical western North Pacific features northeasterlies. There is a dominance of equatorward flow along the upwelling regions along the west coasts of the Americas and Africa, which is associated with the mean anticyclonic circulation in the eastern parts of the respective ocean basins (see Fig. 3a). The tongue of southwesterlies in the equatorial eastern Pacific (Fig. 6) is associated with the position of the intertropical convergence zone (ITCZ; e.g., Schneider et al. 2014) and the tongue of lower SSTs (see Fig. 2c).

Westerlies dominate the midlatitudes, due to the mean zonal flow associated with the eddy-driven jet. A notable exception is the western North Pacific featuring northwesterlies associated with the Asian winter monsoon (Wang and Chen 2014). The higher latitudes in the Northern Hemisphere are dominated by northerlies and northeasterlies associated with cold air outbreaks (e.g., Papritz and

Spengler 2017), where cold and dry air masses with continental or sea ice origin move over the open ocean. The more varied signal around India is due to the Asian monsoon (Ding and Chan 2005) and will be explained in further detail in section 5b where we discuss the seasonality.

For 6-hourly data, the ratio of the heat flux explained by the wind direction is ~60% and ~40% in the tropical and midlatitude region, respectively (contours in Figs. 6a,c). The results in the low latitudes between 30°N and 30°S are almost unaltered compared to the monthly mean data. In the midlatitudes, however, the results change drastically compared to the monthly mean data and the wind direction has an equatorward component in both hemispheres. The equatorward component is most likely associated with the orientation of cold fronts and cold air outbreaks in these regions, which have been hypothesized to play a crucial role for air–sea interactions along the regions of higher SST gradients (e.g., Iwasaki et al. 2014; Parfitt et al. 2016; Vanniere et al. 2017a, b; Zolina and Gulev 2003).

There is a notable difference in direction between SSHF and SLHF in the midlatitudes of the Southern
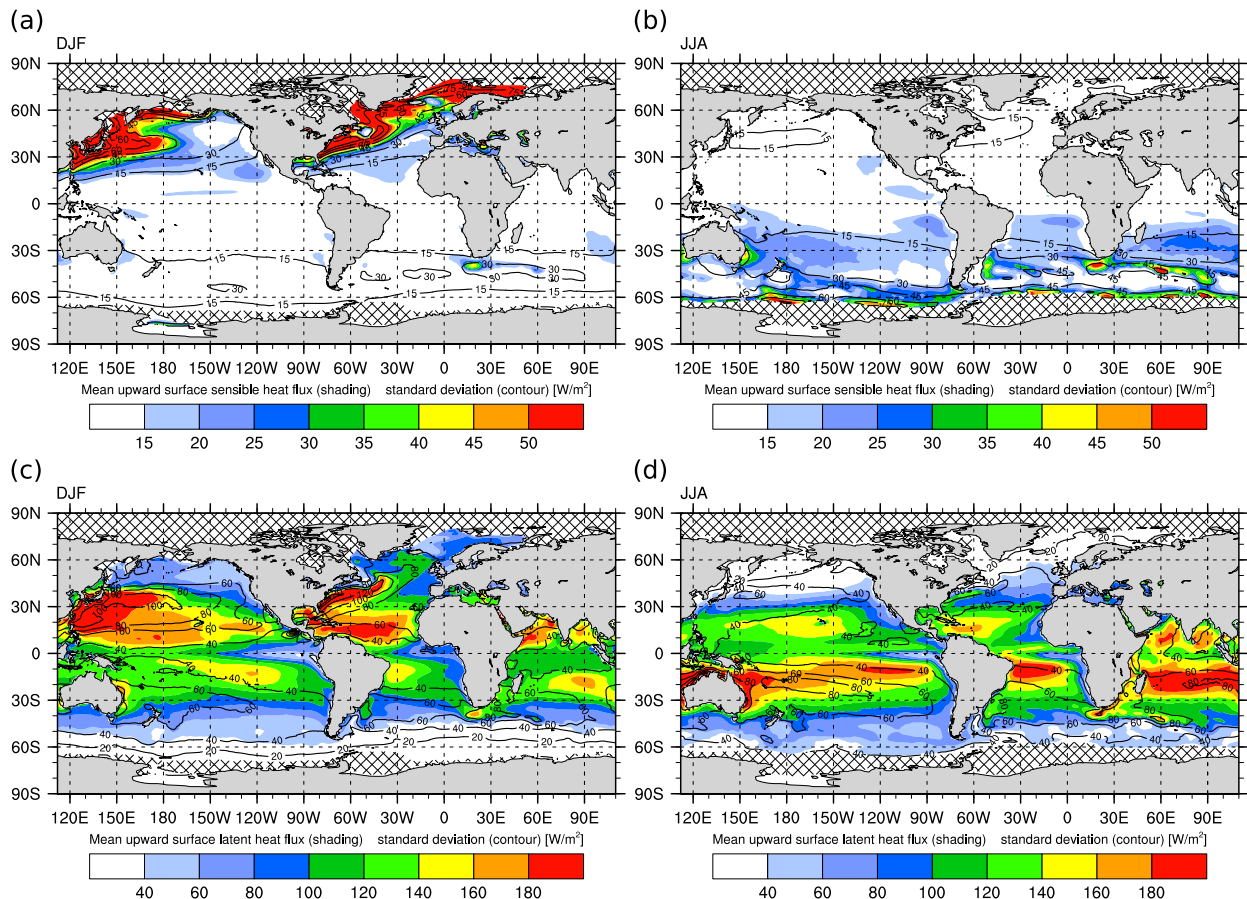
FIG. 7. Mean upward surface sensible (a),(b) and latent (c),(d) heat flux (W m^{-2}; shading) and their standard deviation (W m^{-2}; contours) for (left) DJF and (right) JJA.

Hemisphere for 6-hourly data. While the SSHF is dominated by southwesterlies (Fig. 6a), the SLHF has a westerly wind component over larger areas (Fig. 6c). The westerlies in SLHF are most evident poleward of the SST front in the Southern Hemisphere. The lack of a northward component is most likely due to the low temperature associated with equatorward flow from Antarctica. According to the Clausius–Clapeyron relation, the atmospheric saturation humidity decreases exponentially with temperatures, which results in a significantly reduced uptake potential of SLHF at lower temperatures (see also discussion in Papritz and Spengler 2017). Hence, the cold air mass from Antarctica must first undergo a transformation via sensible heating, which occurs while the flow is turning cyclonically in the cold sector of the cyclone, yielding a more eastward flow component by the time when the warmed airmass can take up significant amounts of latent heat.

b. Seasonal dependence

SSHF and SLHF feature a distinct seasonal cycle with largest fluxes in the respective winter hemisphere

(Fig. 7). It is evident that the dominant contribution of the signal in the annual mean SSHF and SLHF (Fig. 1) originates from the respective wintertime fluxes. The seasonal differences are more pronounced for the SSHF (Figs. 7a,b) compared to the SLHF (Figs. 7c,d), though both SSHF and SLHF differ by an order of magnitude between DJF and JJA in the regions of the Northern Hemisphere SST fronts along the Gulf Stream and Kuroshio. In the Southern Hemisphere storm track, SSHF is about 50% larger in winter (JJA) compared to summer (DJF). The SLHF varies little in the Southern Hemisphere and the low latitudes, the only notable regions of seasonality being between 10° and 30°S and along the SST front in the Southern Indian Ocean.

Another striking difference between the SSHF and the SLHF is evident along the sea ice edge, featuring a strong seasonality in SSHF with largest fluxes in winter, whereas the winter SLHF is only slightly elevated compared to its summer values. This difference was explained above following arguments by Papritz and Spengler (2017). This contrast helps to interpret the seasonality more generally, where the wintertime cold
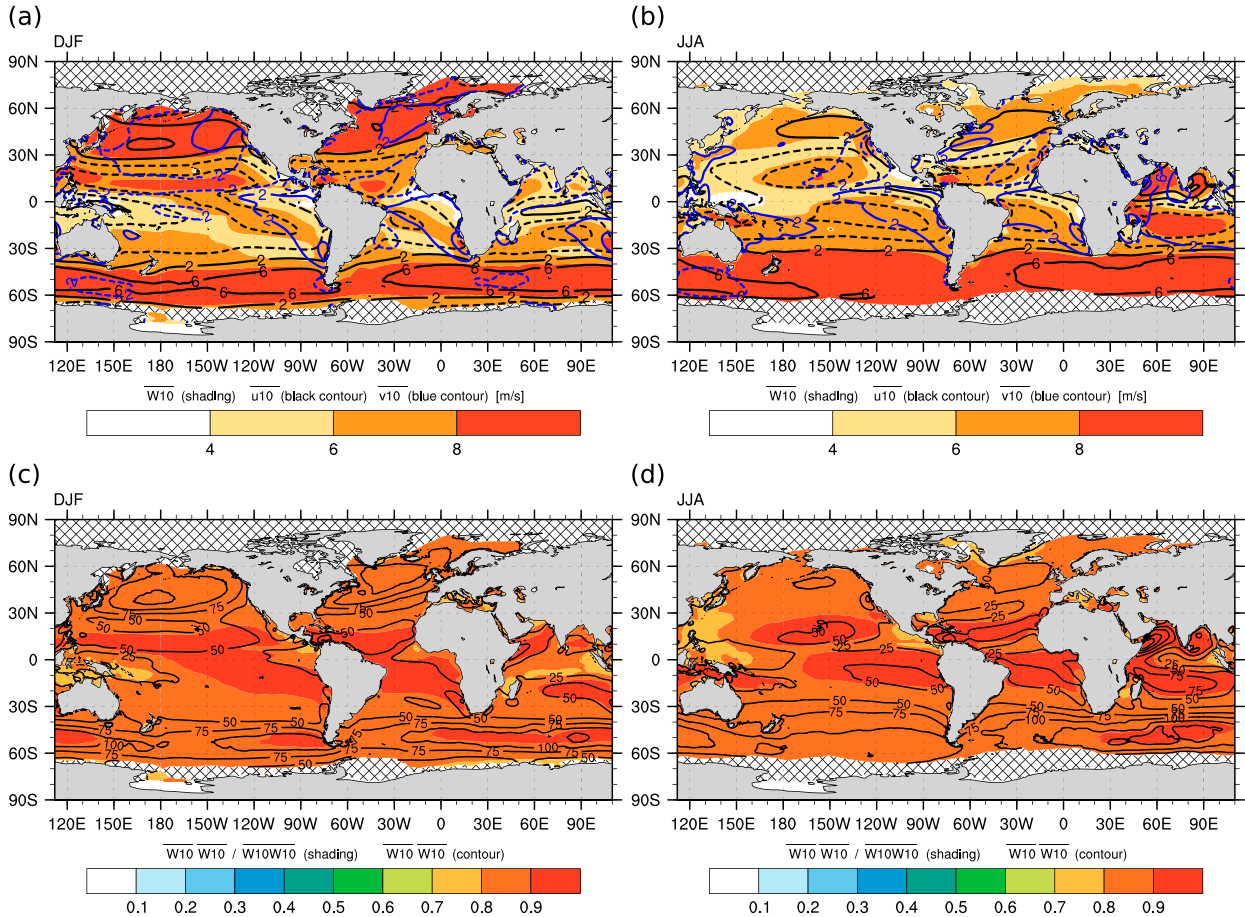
FIG. 8. Decomposition of the mean wind for (left) DJF and (right) JJA for (a),(b) mean wind $\overline{w}_{10}$ (m s^{-1}; shading) and mean wind components $\overline{u}_{10}$ (m s^{-1}; black contours) and $\overline{v}_{10}$ (m s^{-1}; blue contours) and (c),(d) the ratio $\overline{w}_{10}^2/\overline{w_{10}^2}$ (shading) and $\overline{w}_{10}^2$ (m^2 s^{-2}; contours).

and dry air of continental or sea ice origin leads to largest SSHF along the coastal margins in the Northern Hemisphere and Antarctica. The Southern Ocean, on the other hand, has no equivalent cold and dry continental margins and thus the contrast in air masses is diminished, yielding overall reduced SSHF and seasonality.

Similar to the annual mean statistics, $\overline{w}_{10}^2$ explains more than 80% of $\overline{w_{10}^2}$ for both DJF and JJA (cf. Fig. 3c with Figs. 8c,d). The time-mean wind components dominate the low latitudes and the eddies dominate the midlatitudes with 60%–90%, respectively (cf. Figs. 3d,f with Fig. 9). In addition, the ratio of the mean submonthly eddies compared to the mean wind is enhanced over the eastern ocean basins in both summer hemispheres, corresponding to the center of the high pressure system (dashed lines in Figs. 9c and 9d). In the winter hemispheres, the ratio is enhanced along 30° latitude, corresponding to the subtropical high pressure belts. The higher ratio in winter is more apparent in the

Southern Hemisphere, concomitant with the seasonally enhanced subtropical SST gradient (Miyamoto et al. 2018). While the maximum ratio is found in collocation with the storm tracks in the western part of the mid-latitude ocean basins, the subtropical maxima are found in collocation with the climatological high pressure systems in the middle or eastern part of the ocean basins. The tropical western Pacific Ocean also features a larger eddy contribution, due to both lower time-mean winds (Fig. 3a) as well as enhanced eddy activity (Fig. 3b). The submonthly eddy activity in this area is most likely associated with the Madden–Julian oscillation (MJO; e.g., Madden and Julian 1994).

Comparing the dominant wind directions for SSHF (Fig. 10) and SLHF (Fig. 11) in summer and winter to the annual mean (Fig. 6) for both 6-hourly and monthly mean data, it is obvious that the annual midlatitude signal is dominated by the respective winter hemisphere. This is readily explained by the significantly higher fluxes in the respective winter hemisphere. The annual
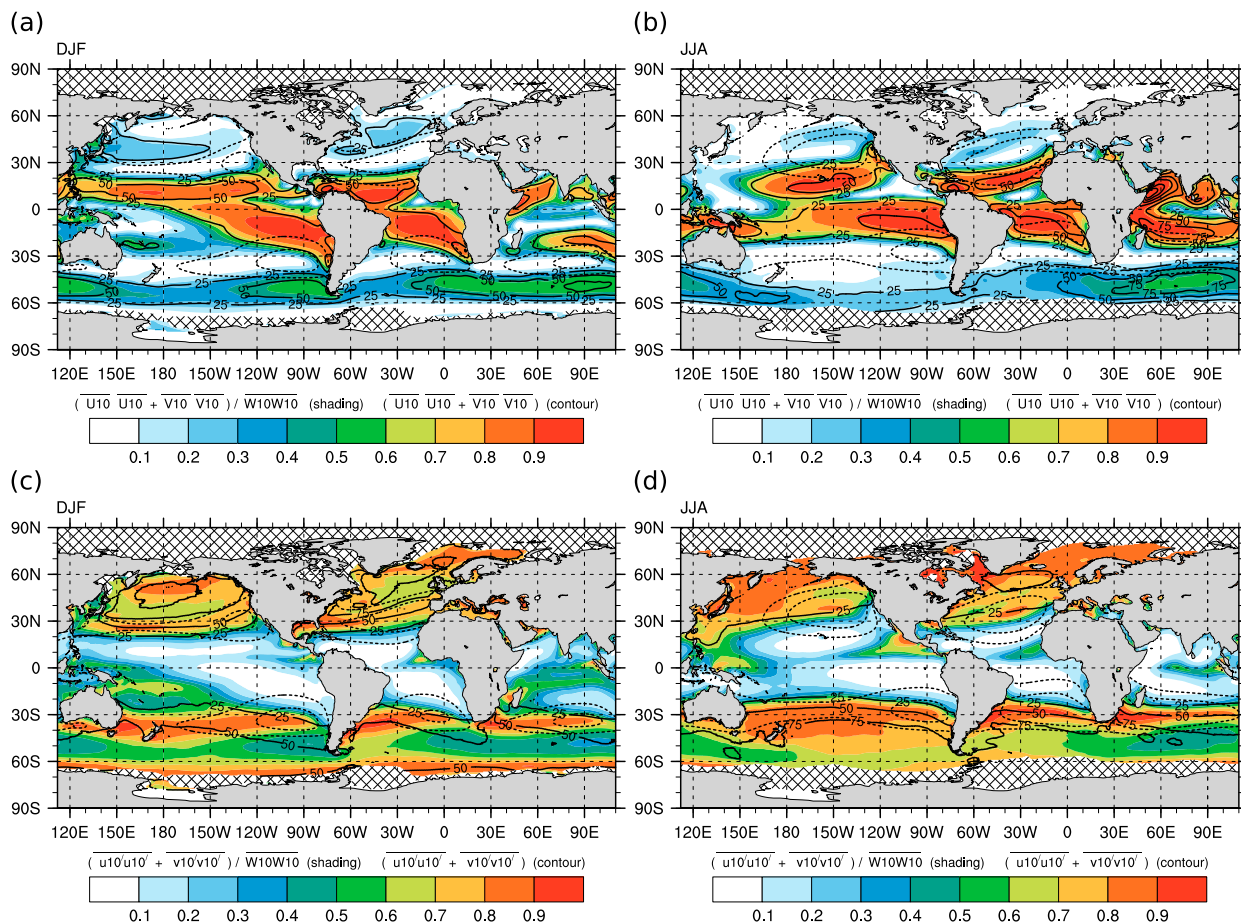
FIG. 9. Ratio for (a),(b) mean wind components $(\overline{u}_{10}^2 + \overline{v}_{10}^2)/\overline{w_{10}^2}$ (shading) and (c),(d) eddy wind components $(\overline{u_{10}'^2} + \overline{v_{10}'^2})/\overline{w_{10}^2}$ (shading), with the sum of the means of the respective wind components for (left) DJF and (right) JJA contours. Dashed contours indicate the climatological seasonal mean sea level pressure (1016 and 1020 hPa, respectively).

mean signal in the tropical and subtropical region in the northern Indian Ocean, on the other hand, is dominated by the Northern Hemisphere summer Asian monsoon (Ding and Chan 2005). This is evident in the JJA mean wind direction during the Asian monsoon, which has a significant southerly component (Fig. 8b). Furthermore, the northwesterly signal around Japan in the annual mean is due to the winter monsoon (Wang and Chen 2014) in the region (Fig. 8a), which is present both in the 6-hourly as well as the monthly mean data (Figs. 10a,c; 11a,c). The DJF westerlies along 10°S in both SSHF and SLHF in the south Indian Ocean and warm pool region are most likely associated with the MJO, which is strongest during DJF and features higher surface westerlies (e.g., Zhang 2005; Shinoda et al. 2013). There are also tongues of southerlies/southwesterlies near the equator in the tropical eastern Pacific and Atlantic. They are more pronounced during JJA and are associated with stronger cross-equatorial flow related to the position of the ITCZ (e.g., Schneider et al. 2014).

The Greenland tip jet (Doyle and Shapiro 1999) has previously been pointed out as a significant wind phenomena around Greenland associated with air–sea interactions (Pickart et al. 2003; Våge et al. 2009). While the tip jet occurrence is significantly higher during DJF compared to JJA (Moore 2003), the structure of the westerlies at the southern tip of Greenland is clearly discernible in the JJA wind direction (Fig. 10b). A similar feature is also evident at the southern tip of the Kamchatka peninsula. Thus, even though the overall fluxes are very low during JJA, they appear to be mainly associated with these regional flow phenomena. During DJF, there are other types of strong wind events that mask out the signature of the tip jets, though the northeasterlies in the northern Bering Sea are consistent with the wind direction of the most intense wind events in the area (Moore and Pickart 2012).

The equatorward and poleward shift of the mean and eddy signatures (Fig. 9) is evident when comparing midlatitude summer and winter for both SSHF and
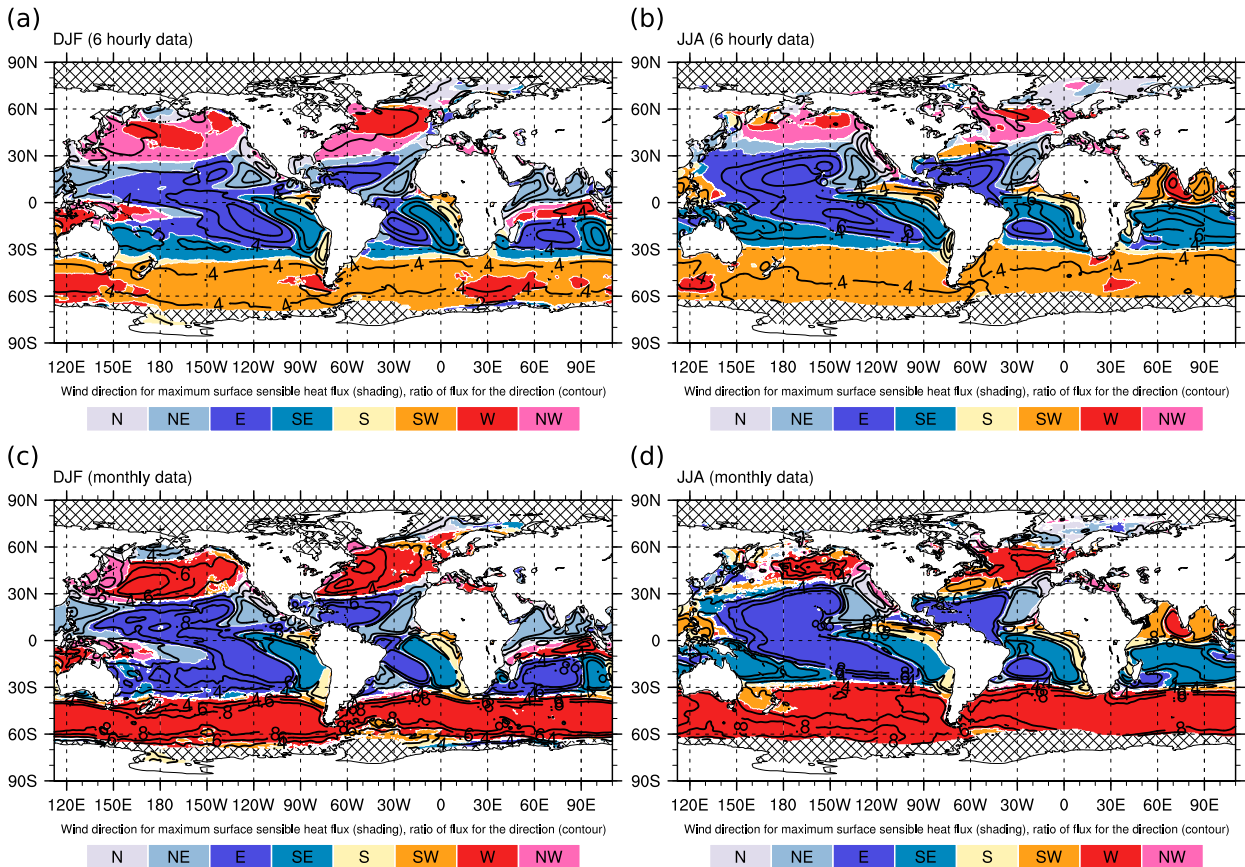
FIG. 10. As Fig. 6, but for surface sensible heat flux in (left) DJF and (right) JJA for (a),(b) 6-hourly and (c),(d) monthly mean data.

SLHF and 6-hourly as well as monthly mean data (Figs. 10, 11). In particular, the regions around the main SST fronts along the Kuroshio and Gulf Stream feature significant seasonal differences. For 6-hourly data, the DJF SSHF and SLHF are dominated by northwesterly flow across the SST front (Figs. 10a, 11a). In summer, however, the meridional component actually reverses sign (see Figs. 8a,b), yielding southwesterlies associated with the summertime anticyclone in the Gulf Stream region, which are in fact evident in both 6-hourly and monthly mean data (Figs. 10b,d, 11b,d). The summertime southwesterlies in the Pacific are only evident in the monthly mean data, whereas the 6-hourly data feature northeasterlies.

This difference between the Pacific and the Atlantic is most likely due to the fact that the North American continent is in close proximity to the SST front along the Gulf Stream. This tight land–sea contrast allows eddies to regularly spill cold and dry air masses across the SST front during winter. In summer, however, the heated continent yields a reversal in land–sea airmass contrast and thus a reduced effect of the eddies on the air–sea heat exchange. In the Pacific, the Asian continent is

significantly farther away from the Kuroshio SST front. Thus, the summertime air masses spilling from the heated continent will first adjust to the underlying SST, still allowing for a significant eddy imprint on the heat exchange across the SST front. Thus, despite the climatological-mean southwesterlies during JJA in the Atlantic and Pacific, the eddies are still dominating in the western midlatitude Pacific, while the mean wind direction dominates in the Atlantic. Another reason for the difference is that the climatological southwesterlies in summer are stronger in the North Atlantic compared to the North Pacific (Fig. 8b). This is also evident in the mean wind components featuring a greater than 30% contribution to $\overline{w_{10}^2}$ in the western North Atlantic near the SST front (Fig. 9b).

6. Concluding remarks

We presented a climatology of prevailing wind direction for upward SSHF and SLHF based on ERA-Interim reanalysis data for the period 1979–2015. Using the bulk formulas, we showed that the time-mean $\overline{\text{SSHF}}$ and $\overline{\text{SLHF}}$ are largely associated with the time-mean
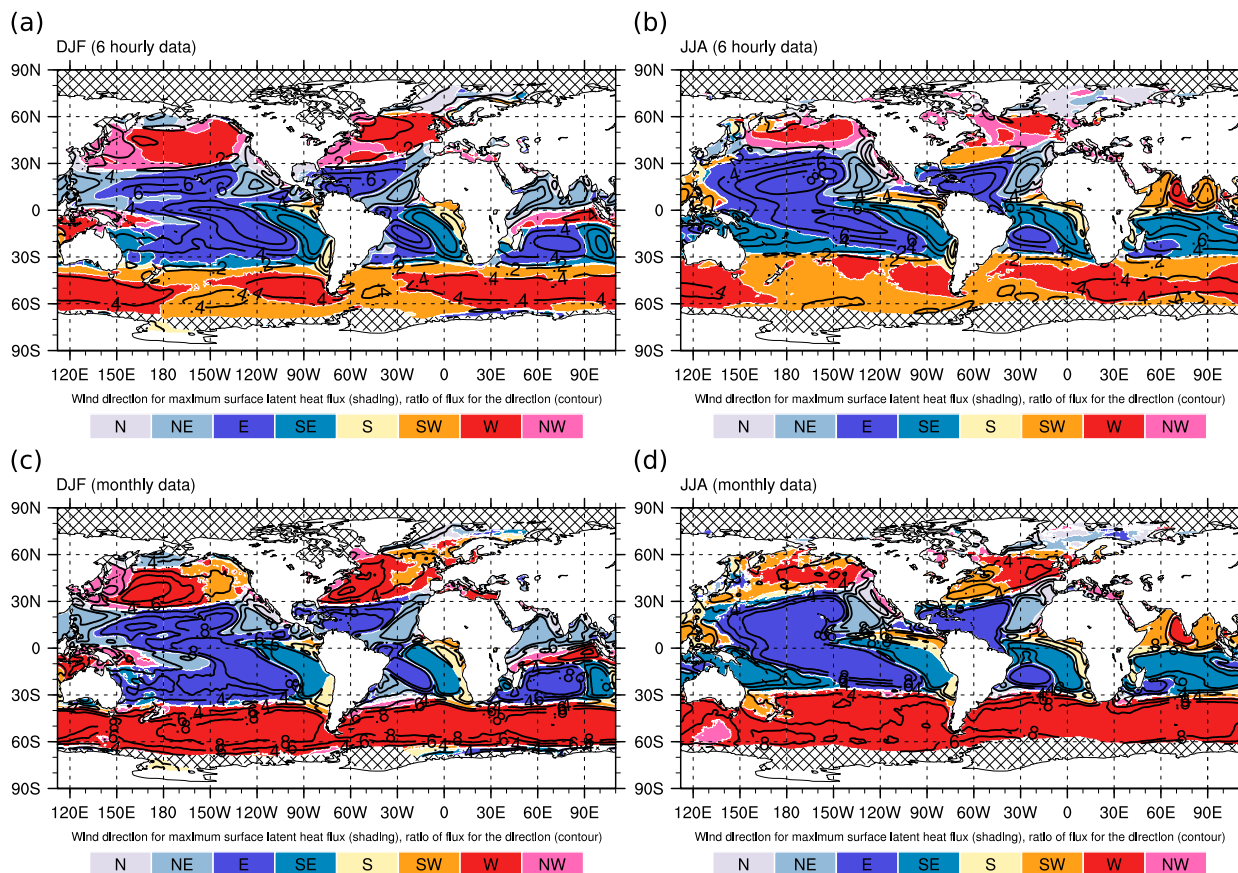
FIG. 11. As Fig. 10, but for surface latent heat flux.

air–sea temperature difference $\overline{\Delta T}$ and difference between atmospheric specific humidity and saturation specific humidity at SST $\overline{\Delta q}$ as well as the time-mean surface wind speed $\overline{w}_{10}$. While $\overline{\Delta T}$ and $\overline{\Delta q}$ are linear, $\overline{w}_{10}$ is nonlinear in the wind components and thus not interpretable as straightforwardly. We illustrated this by separating the mean wind into a time-mean, 30-day running mean, and a submonthly eddy part. While the low latitudes, except for the center of the subtropical high pressure system, are largely dominated by the mean of the zonal and meridional wind components, the midlatitudes are dominated by synoptic-scale eddies.

Motivated by these findings, we binned SSHF and SLHF by the eight main wind directions for instantaneous 6-hourly data, as well as daily, weekly, and monthly mean data, and performed the analysis for the entire period 1979–2015 as well as for the seasons DJF and JJA. We first presented an example for grid points either in the low-latitude western Atlantic or just equatorward of the SST front associated with the Gulf Stream. While we found a striking contrast between the 6-hourly/daily mean and the weekly/monthly mean data for the midlatitude grid points, the low-latitude grid

points featured a similar wind distribution irrespective of the time averaging. The midlatitudes are dominated by equatorward flow across the SST front for the 6-hourly and daily mean data, whereas the weekly and monthly mean results mainly feature westerlies associated with the mean surface westerlies associated with the eddy driven jet. The transition of the prevailing wind direction from northwesterly for daily to westerly for weekly time scales is consistent with the typical time scale that a migrating synoptic cyclone yields a certain wind direction at a given location. In the low latitudes, however, all data show easterlies as the dominant wind direction, consistent with the dominance of the rather stable trade winds reflected in the time-mean wind components.

As the largest fluxes in the midlatitudes occur in the respective winter hemisphere, the results for the annual mean in these latitudes are dominated by the winter season. The winter midlatitudes were also the region with the most striking differences between the 6-hourly and monthly mean fluxes, where the monthly mean is dominated by westerlies along the storm track region, whereas the 6-hourly data feature a distinct equatorward

cross-SST-front wind component. The low latitudes, on the other hand, feature similar fluxes all year around and the annual mean wind direction is mostly dominated by seasonal patterns such as the monsoon circulation in the Asian and Australian regions. Strikingly, there is almost no difference between the 6-hourly and monthly mean wind directions associated with the fluxes in the low latitudes, where both are dominated by the easterly trade winds.

The seasonal differences for the SSHF and SLHF in the midlatitudes show the seasonal poleward and equatorward progression of the storm track. In addition to the meridional shift in the Atlantic Gulf Stream region, the flow shifts from northwesterlies in the winter to southwesterlies in summer for both 6-hourly as well as monthly mean data. Hence, while the fluxes are dominated by a cross-SST-front component from the colder to the warmer side in winter, the associated flow reverses during summer. This contrast is most likely attributable to the land–sea contrast, where the North American continent is rather close to the SST front, while the SST front in the Pacific has no larger continental landmasses nearby. In addition, the North Atlantic features a change in seasonal mean flow associated with an anticyclone in the western midlatitude Atlantic, yielding a more dominant southwesterly flow compared to the Pacific in summer.

The Asian summer monsoon dominates the annual mean flow characteristics in the north Indian Ocean with southwesterly flow in JJA and westerners along the east coast of India, whereas the Asian winter monsoon has a significant imprint on the northwesterly flow around Japan in the northwestern Pacific. The flow direction associated with the fluxes in the low latitudes is mostly influenced by the trade winds, while the equatorial region has an imprint of westerlies in the warm pool region during DJF due to the MJO and the eastern equatorial regions in the Pacific and Atlantic feature southwesterlies associated with the position of the ITCZ.

Our analysis shows that the prevailing wind direction associated with air–sea heat exchange in the low latitudes does not significantly depend on the time averaging. The mean wind speed and direction largely determine the prevailing wind direction for surface fluxes in these regions. This allows for a more general interpretation of the fluxes based on time-mean fields and linear theory assuming stationarity.

In the midlatitudes, however, there is a striking contrast in the wind direction associated with the fluxes depending on time averaging of the data. Based on the 6-hourly data, the largest midlatitude upward heat fluxes are associated with equatorward flow connected to synoptic eddies that advect cold and dry air across the SST
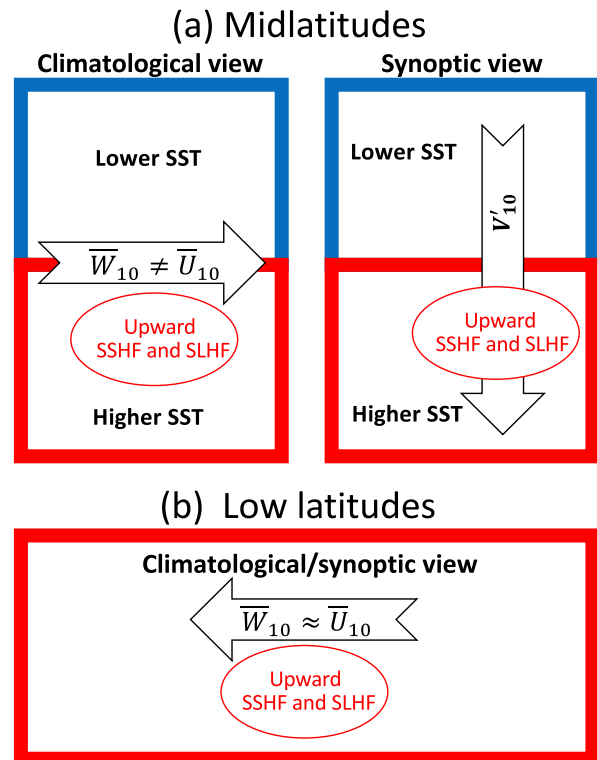

FIG. 12. Schematic illustrating the climatological and synoptic interpretations of the surface heat fluxes for the (a) midlatitudes and (b) low latitudes. Although the two interpretations align in the low latitudes, the climatological and synoptic viewpoint in the midlatitudes is distinct, highlighting the role of the synoptic eddies to understand the fluxes along the midlatitude SST fronts.

fronts. The importance of these midlatitude equatorward wind components for the 6-hourly and daily data pinpoint the necessity to consider subweekly synoptic-scale eddies for the climatological interpretation of the mean surface fluxes in the midlatitudes. Thus, associating air–sea fluxes with wind directions using low-pass-filtered or time-mean data with cutoff periods beyond time scales of subweekly eddies that exclude baroclinic cyclone development is misleading. A similar importance of the meridional flow is found along the sea ice edge, where episodic cold air outbreaks lead to an equatorward wind component.

Overall, due to the dominance of the mean wind components to the climatological-mean wind speed in the subtropical and tropical latitudes, the climatological and synoptic view yield an identical interpretation with fluxes mainly associated with surface easterlies (Fig. 12b). This also implies that linear steady-state theory for air–sea heat exchange provides physically meaningful results in this area. For the midlatitudes, however, we found that the subweekly eddies dominate the climatological-mean wind speed and one must thus employ frameworks that allow for the effects of transient subweekly synoptic

eddies when investigating midlatitude air–sea heat exchange. The climatological view with surface westerlies along the major midlatitude SST fronts does thus not provide a physically meaningful interpretation. The synoptic view with significant meridional flow across the SST fronts, in contrast, provides a physically straightforward explanation of the high air–sea heat fluxes in these regions (Fig. 12a). Our results, thus, support recent studies highlighting the importance of episodic synoptic events and the passage of atmospheric fronts along the midlatitude SST fronts for the climatological-mean state in these regions. Our findings also have implications for the coupling time step in Earth system models. For example, while forcing an ocean model with average atmospheric fields might yield the correct climatological-mean surface heat fluxes, the physicality is infringed, as the fluxes are actually associated with meridional excursions of cold air across the SST front.

REFERENCES

Berry, G., M. J. Reeder, and C. Jakob, 2011: A global climatology of atmospheric fronts. *Geophys. Res. Lett.*, **38**, L04809, https://doi.org/10.1029/2010GL046451.

Booth, J. F., L. Thompson, J. Patoux, K. A. Kelly, and S. Dickinson, 2010: The signature of the midlatitude tropospheric storm tracks in the surface winds. *J. Climate*, **23**, 1160–1174, https://doi.org/10.1175/2009JCLI3064.1.

——, ——, ——, and ——, 2012: Sensitivity of midlatitude storm intensification to perturbations in the sea surface temperature near the Gulf Stream. *Mon. Wea. Rev.*, **140**, 1241–1256, https://doi.org/10.1175/MWR-D-11-00195.1.

Brayshaw, D. J., B. Hoskins, and M. Blackburn, 2009: The basic ingredients of the North Atlantic storm track. Part I: Land–sea contrast and orography. *J. Atmos. Sci.*, **66**, 2539–2558, https://doi.org/10.1175/2009JAS3078.1.

Czaja, A., and N. Blunt, 2011: A new mechanism for ocean–atmosphere coupling in midlatitudes. *Quart. J. Roy. Meteor. Soc.*, **137**, 1095–1101, https://doi.org/10.1002/qj.814.

Dee, D. P., and Coauthors, 2011: The ERA-Interim reanalysis: Configuration and performance of the data assimilation system. *Quart. J. Roy. Meteor. Soc.*, **137**, 553–587, https://doi.org/10.1002/qj.828.

Ding, Y., and J. C. L. Chan, 2005: The East Asian summer monsoon: An overview. *Meteor. Atmos. Phys.*, **89**, 117–142, https://doi.org/10.1007/S00703-005-0125-z.

Doyle, J. D., and M. A. Shapiro, 1999: Flow response to large-scale topography: The Greenland tip jet. *Tellus*, **51A**, 728–748, https://doi.org/10.3402/tellusa.v51i5.14471.

Hartmann, D., 1994: *Global Physical Climatology*. Academic Press, 411 pp.

Hoskins, B. J., and K. I. Hodges, 2002: New perspectives on the Northern Hemisphere winter storm tracks. *J. Atmos. Sci.*, **59**, 1041–1061, https://doi.org/10.1175/1520-0469(2002)059<1041:NPOTNH>2.0.CO;2.

Hotta, D., and H. Nakamura, 2011: On the significance of sensible heat supply from the ocean in the maintenance of mean baroclinicity along storm tracks. *J. Climate*, **24**, 3377–3401, https://doi.org/10.1175/2010JCLI3910.1.

Iwasaki, T., T. Shoji, Y. Kanno, M. Sawada, M. Ujiie, and K. Takaya, 2014: Isentropic analysis of polar cold airmass streams in the Northern Hemisphere winter. *J. Atmos. Sci.*, **71**, 2230–3342, https://doi.org/10.1175/JAS-D-13-058.1.

Kobayashi, S., and Coauthors, 2015: The JRA-55 Reanalysis: General specifications and basic characteristics. *J. Meteor. Soc. Japan*, **93**, 5–48, https://doi.org/10.2151/jmsj.2015-001.

Lambaerts, J., G. Lapeyre, R. Plougonven, and P. Klein, 2013: Atmospheric response to sea surface temperature mesoscale structures. *J. Geophys. Res.*, **118**, 9611–9621, https://doi.org/10.1002/JGRD.50769.

Lindzen, R. S., and S. Nigam, 1987: On the role of sea surface temperature gradients in forcing low-level winds and congence in the Tropics. *J. Atmos. Sci.*, **44**, 2418–2436, https://doi.org/10.1175/1520-0469(1987)044<2418:OTROSS>2.0.CO;2.

Madden, R. A., and P. R. Julian, 1994: Observations of the 40–50-day tropical oscillation—A review. *Mon. Wea. Rev.*, **122**, 814–837, https://doi.org/10.1175/1520-0493(1994)122<0814:OOTDTO>2.0.CO;2.

Masunaga, R., H. Nakamura, T. Miyasaka, K. Nishii, and Y. Tanimoto, 2015: Separation of climatological imprints of the Kuroshio Extension and Oyashio Fronts on the wintertime atmospheric boundary layer: Their sensitivity to SST resolution prescribed for atmospheric reanalysis. *J. Climate*, **28**, 1764–1787, https://doi.org/10.1175/JCLI-D-14-00314.1.

Minobe, S., A. Kuwano-Yoshida, N. Komori, S.-P. Xie, and R. J. Small, 2008: Influence of the Gulf Stream on the troposphere. *Nature*, **452**, 206–210, https://doi.org/10.1038/nature06690.

——, M. Miyashita, A. Kuwano-Yoshida, H. Tokinaga, and S.-P. Xie, 2010: Atmospheric response to the Gulf Stream: Seasonal variations. *J. Climate*, **23**, 3699–3719, https://doi.org/10.1175/2010JCLI3359.1.

Miyamoto, A., H. Nakamura, and T. Miyasaka, 2018: Influence of the subtropical high and storm track on low-cloud fraction and its seasonality over the South Indian Ocean. *J. Climate*, **31**, 4017–4039, https://doi.org/10.1175/JCLI-D-17-0229.1.

Moore, G. W. K., 2003: Gale force winds over the Irminger Sea to the east of Cape Farewell, Greenland. *Geophys. Res. Lett.*, **30**, 1894, https://doi.org/10.1029/2003GL018012.

——, and R. S. Pickart, 2012: Northern Bering Sea tip jets. *Geophys. Res. Lett.*, **39**, L08807, https://doi.org/10.1029/2012GL051537.

Nakamura, H., T. Sampe, Y. Tanimoto, and A. Shimpo, 2004: Observed associations among storm tracks, jet streams and midlatitude oceanic fronts. *Earth's Climate: The Ocean–Atmosphere Interaction*, *Geophys. Monogr.*, Vol. 147, Amer. Geophys. Union, 329–345, https://doi.org/10.1029/147GM18.

Nonaka, M., H. Nakamura, B. Taguchi, N. Komori, A. Yoshida-Kuwano, and K. Takaya, 2009: Air–sea heat exchanges characteristic to a prominent midlatitude oceanic front in the South Indian Ocean as simulated in a high-resolution coupled GCM. *J. Climate*, **22**, 6515–6535, https://doi.org/10.1175/2009JCLI2960.1.

Ogawa, F., H. Nakamura, K. Nishii, T. Miyasaka, and A. Kuwano-Yoshida, 2012: Dependence of the climatological axial latitudes of the tropospheric westerlies and storm tracks on the latitude of an extratropical oceanic front. *Geophys. Res. Lett.*, **35**, L15709, https://doi.org/10.1029/2011GL049922.

O'Neill, L., T. Haack, D. B. Chelton, and E. Skyllingstad, 2017: The Gulf Stream convergence zone in the time-mean winds. *J. Atmos. Sci.*, **74**, 2383–2412, https://doi.org/10.1175/JAS-D-16-0213.1.

Papritz, L., and T. Spengler, 2015: Analysis of the slope of isentropic surfaces and its tendencies over the North Atlantic. *Quart. J. Roy. Meteor. Soc.*, **141**, 3226–3238, https://doi.org/10.1002/qj.2605

——, and ——, 2017: A Lagrangian climatology of wintertime cold air outbreaks in the Irminger and Nordic Seas and their role in shaping air–sea heat fluxes. *J. Climate*, **30**, 2717–2737, https://doi.org/10.1175/JCLI-D-16-0605.1.

Parfitt, R., and A. Czaja, 2016: On the contribution of synoptic transients to the mean atmospheric state the Gulf Stream region. *Quart. J. Roy. Meteor. Soc.*, **142**, 1554–1561, https://doi.org/10.1002/qj.2689.

——, and H. Seo, 2018: A new framework for near-surface wind convergence over the Kuroshio Extension and Gulf Stream in wintertime: The role of atmospheric fronts. *Geophys. Res. Lett.*, **45**, 9909–9918, https://doi.org/10.1029/2018GL080135.

——, A. Czaja, S. Minobe, and A. Kuwano-Yoshida, 2016: The atmospheric frontal response to SST perturbations in the Gulf Stream region. *Geophys. Res. Lett.*, **43**, 2299–2306, https://doi.org/10.1002/2016GL067723.

Peixoto, J. P., and A. H. Oort, 1992: *Physics of Climate*. 1st ed. American Institute of Physics, 520 pp.

Pickart, R. S., M. A. Spall, M. H. Ribergaard, G. W. K. Moore, and R. F. Milliff, 2003: Deep convection in the Irminger Sea forced by the Greenland tip jet. *Nature*, **424**, 152–156, https://doi.org/10.1038/nature01729.

Sampe, T., H. Nakamura, A. Goto, and W. Ohfuchi, 2010: Significance of a midlatitude SST frontal zone in the formation of a storm track and an eddy-driven westerly jet. *J. Climate*, **23**, 1793–1814, https://doi.org/10.1175/2009JCLI3163.1.

Schneider, T., T. Bischoff, and G. H. Haug, 2014: Migrations and dynamics of the intertropical convergence zone. *Nature*, **513**, 45–53, https://doi.org/10.1038/nature13636.

Shinoda, T., T. G. Jensen, M. Flatau, and S. Chen, 2013: Surface wind and upper-ocean variability associated with the Madden–Julian oscillation simulated by the Coupled Ocean–Atmosphere Mesoscale Prediction System (COAMPS). *Mon.*

Wea. Rev., **141**, 2290–2307, https://doi.org/10.1175/MWR-D-12-00273.1.

Simmonds, I., and M. Dix, 1989: The use of mean atmospheric parameters in the calculation of modeled mean surface heat fluxes over the world's oceans. *J. Phys. Oceanogr.*, **19**, 205–215, https://doi.org/10.1175/1520-0485(1989)019<0205:TUOMAP>2.0.CO;2.

Taguchi, B., H. Nakamura, M. Nonaka, and S. P. Xie, 2009: Influences of the Kuroshio/Oyashio Extensions on air–sea heat exchanges and storm track activity as revealed in regional atmospheric model simulations for the 2003/04 cold season. *J. Climate*, **22**, 6536–6560, https://doi.org/10.1175/2009JCLI2910.1.

Tilinina, N., A. Gavrikov, and S. K. Gulev, 2018: Association of the North Atlantic surface turbulent heat fluxes with midlatitude cyclones. *Mon. Wea. Rev.*, **146**, 3691–3715, https://doi.org/10.1175/MWR-D-17-0291.1.

Våge, K., T. Spengler, H. C. Davies, and R. S. Pickart, 2009: Multi-event analysis of the westerly Greenland tip jet based upon 45 winters in ERA-40. *Quart. J. Roy. Meteor. Soc.*, **135**, 1999–2011, https://doi.org/10.1002/qj.488.

Vallis, G. K., 2017: *Atmospheric and Oceanic Fluid Dynamics*. 2nd ed. Cambridge University Press, 946 pp.

Vanniere, B., A. Czaja, and H. F. Dacre, 2017a: Contribution of the cold sector of extratropical cyclones to mean state features over the Gulf Stream in winter. *Quart. J. Roy. Meteor. Soc.*, **143**, 1990–2000, https://doi.org/10.1002/qj.3058.

——, ——, ——, and T. Woollings, 2017b: A "cold path" for the Gulf Stream–troposphere connection. *J. Climate*, **30**, 1363–1379, https://doi.org/10.1175/JCLI-D-15-0749.1.

Vincent, D. G., 1994: The South Pacific convergence zone (SPCZ): A review. *Mon. Wea. Rev.*, **122**, 1949–1979, https://doi.org/10.1175/1520-0493(1994)122<1949:TSPCZA>2.0.CO;2.

Wallace, J. M., T. Mitchell, and C. Deser, 1989: The influence of sea surface temperature on surface wind in the eastern equatorial Pacific: Seasonal and interannual variability. *J. Climate*, **2**, 1492–1499, https://doi.org/10.1175/1520-0442(1989)002<1492:TIOSST>2.0.CO;2.

Wang, L., and W. Chen, 2014: An intensity index for the East Asian winter monsoon. *J. Climate*, **27**, 2361–2374, https://doi.org/10.1175/JCLI-D-13-00086.1.

Xie, S. P., 2004: Satellite observations of cool ocean–atmosphere interaction. *Bull. Amer. Meteor. Soc.*, **85**, 195–2008, https://doi.org/10.1175/BAMS-85-2-195.

Zhang, C., 2005: Madden–Julian oscillation. *Rev. Geophys.*, **43**, RG2003, https://doi.org/10.1029/2004RG000158.

Zolina, O., and S. Gulev, 2003: Synoptic variability of ocean–atmosphere turbulent fluxes associated with atmospheric cyclones. *J. Climate*, **16**, 2717–2734, https://doi.org/10.1175/1520-0442(2003)016<2717:SVOOTF>2.0.CO;2.